Brazilian Journal of Physics
ISSN: 0103-9733
luizno.bjp@gmail.com
Sociedade Brasileira de Física
Brasil

Oliveira Dantas, Noelio; Oliveira Serqueira, Elias; Almeida Silva, Anielle Christine; Andrade, Acácio Aparecido; Alves Lourenço, Sidney
High Quantum Efficiency of Nd3+ Ions in a Phosphate Glass System using the Judd–Ofelt Theory
Brazilian Journal of Physics, vol. 43, núm. 4, agosto, 2013, pp. 230-238
Sociedade Brasileira de Física
São Paulo, Brasil

Braz J Phys (2013) 43:230–238
DOI 10.1007/s13538-013-0145-y

CONDENSED MATTER

High Quantum Efficiency of Nd^{3+} Ions in a Phosphate Glass System using the Judd–Ofelt Theory

Noelio Oliveira Dantas · Elias Oliveira Serqueira · Anielle Christine Almeida Silva · Acácio Aparecido Andrade · Sidney Alves Lourenço

Received: 5 August 2012 / Published online: 9 July 2013

Abstract The optical properties of trivalent neodymium embedded in a P_2O_5–Al_2O_3–Na_2O–K_2O phosphate glass system, synthesized by the fusion method, are studied. Absorption, luminescence, lifetime, and Raman spectroscopy measurements were performed and the Judd–Ofelt theory was applied to determine optical parameters such as the quantum efficiency and the stimulated emission cross section of the Nd^{3+}-doped glass system. This structure has high quantum efficiency at low Nd^{3+} concentrations, comparable to the efficiency of a commercial YAG:Nd^{3+} crystal. We discuss the mechanisms responsible for the high quantum efficiency observed in the proposed phosphate glass system.

Keywords High quantum efficiency · Nd^{3+} ions · Phosphate glass system · Judd–Ofelt Theory

1 Introduction

In recent decades, glass systems doped with rare earth (RE) ions have attracted attention due to their mechanical stability, low cost, low conductivity, and thermal properties that are desirable in optical devices with diverse applications [1–6].

Neodymium is the most widely studied doping agent because of its use in neodymium lasers that are highly efficient, even at room temperature [7–9]. However, non-radiative energy transfer by cross relaxation between Nd^{3+} ions, phonon charge losses to the glass network, and energy transfer from Nd^{3+} ions to OH^- and CH radicals reduce quantum efficiency and are obstacles to the development more efficient systems [10–12]. Several researchers have pointed out that SiO_2 is not a suitable host because rare earth ions in the glass tend to form clusters in the silica network. These clusters cause quenching of luminescence due to energy transfer between neighboring ions [10, 11]. Thus, researchers continue to develop new glass systems, with different spectroscopic parameters, for optical device applications [12–15].

In this paper, we report the optical properties of Nd^{3+} ions embedded in a PANK (P_2O_5–Al_2O_3–Na_2O–K_2O) phosphate glass system synthetized by the fusion method at different Nd^{3+} concentrations. Absorption, luminescence, lifetime, and Raman spectroscopy measurements were performed, and the Judd–Ofelt theory [16, 17] was applied to determine optical parameters such as quantum efficiency and the stimulated emission cross section of the Nd^{3+}-doped glass system. The proposed Nd^{3+}-doped PANK glass system has high quantum efficiency at low Nd^{3+} concentrations, and the fluorescence lifetime and quantum efficiency of the $^4F_{3/2}$ state decrease as the Nd^{3+} concentration increases.

2 Theoretical Details

The Judd–Ofelt (JO) theory has been used as a fundamental framework for quantitative spectroscopic analysis of RE ions embedded in different environments. According to

N. O. Dantas (✉) · E. O. Serqueira · A. C. A. Silva
Laboratório de Novos Materiais Isolantes e Semicondutores (LNMIS), Instituto de Física, Universidade Federal de Uberlândia, CP 593, 38400-902 Uberlândia, MG, Brazil
e-mail: noelio@ufu.br

A. A. Andrade
Grupo de Propriedades Ópticas e Térmicas de Materiais (GPOTM), Instituto de Física, Universidade Federal de Uberlândia, CP 593, 38400-902 Uberlândia, MG, Brazil

S. A. Lourenço
Universidade Tecnológica Federal do Paraná, 86036-370 Londrina, PR, Brazil

the Judd–Ofelt theory, electric dipole oscillator strength between electronic transitions from initial $\langle f^N \alpha SLJ|$ to final state $|f^N \alpha S'L'J'\rangle$ can be expressed as [16, 17]

$$f^{ED}(J,J') = \frac{8\pi^2 mc}{3h}\frac{E}{(2J+1)}\chi\sum_{\lambda=2,4,6}\Omega_\lambda\left|\langle f^N aSLJ\left|U^{(\lambda)}\right|f^N\alpha' S'L'J'\rangle\right|^2 \quad (1)$$

where m is electron mass, c is the speed of light, E is the electronic transition energy, h is Planck's constant, J is the angular moment of the initial state $\langle f^N \alpha SLJ|$, $\chi=(n^2+2)^2/(9n)$ is the central field correction factor, n is the refraction index at wavenumber E, Ω_λ is the Judd–Ofelt intensity parameter, and $|\langle f^N \alpha SLJ|U^{(\lambda)}|f^N\alpha' S'L'J'\rangle|^2$ is the reduced matrix element of the tensor operator $U^{(\lambda)}$ obtained from the Carnall et al. calculation [18–20].

The JO intensity parameters Ω_λ (λ=2, 4, 6) can be used to estimate optical quantities such as spontaneous emission probability (AJ, J'), branching ratio ($\beta(J, J')$), stimulated emission cross section ($\sigma(J, J')$), radiative lifetime ($\tau_R(J, J')$), and quantum efficiency (η). These parameters can then be used to predetermine if an RE ion host material is favorable for optical device applications [12, 13]. The Ω_2 parameter, for example, is related to covalency between RE^{3+} ions and ligand anions in the glass environment. It is also associated with the asymmetry of the local environment around RE^{3+} ions. Low values of Ω_2 indicate higher symmetry and higher ionicity of the ligand chemical bonds [21–28].

Judd–Ofelt parameters, Ω_λ (λ=2, 4, 6) can be experimentally obtained from experimental oscillator strenghts via the expression

$$f^{\exp}(\lambda) = \frac{mc}{\pi\ e^2 N}\int \alpha(\lambda)d\lambda\,, \quad (2)$$

where N is the RE ion concentration per unit volume (ions per cubic centimeter), and $\alpha(\lambda)$ is the absorption coefficient. Using Eq. (2) with Eq. (1), it is possible to obtain Ω_λ.

The Ω_λ parameters can then be used to calculate radiative transition rates (AJ, J') with the expression

$$A(J,J') = \frac{64\ \pi^4 e^2}{3h(2J+1)\lambda^3}\chi\sum_{\lambda=2,4,6}\Omega_\lambda\left|\langle f^N\alpha SLJ\left|U^{(\lambda)}\right|f^N\alpha' S'L'J'\rangle\right|^2 \quad (3)$$

The radiative lifetime τ_R of the emission state is given as $\tau_R = 1/\sum_{J'} A(J, J')$.

The emission branching ratio for transitions originating from the initial manifold is related to the radiative transition rates, $A(J,J)'$, by the following equation [1, 12, 13]:

$$\beta\left({}^4F_{3/2}\rightarrow {}^4I_{J'}\right) = \frac{A\left({}^4F_{3/2}\rightarrow {}^4I_{J'}\right)}{\sum_{J'} A\left({}^4F_{3/2}\rightarrow {}^4I_{J'}\right)} \quad (4)$$

where the summation includes each J'(J'=9/2, 11/2, 13/2, and 15/2).

To compare theoretical data obtained from Eq. (4) with experimental data, the ratio of the integral of an emission band, $\int I(\lambda)d\lambda$, to the sum of the integrals of all emission bands, $\sum\int I(\lambda)d\lambda$, is calculated. This results in the experimental emission branching ratio represented by $\beta_{\exp}=\int I(\lambda)d\lambda/\sum\int I(\lambda)d\lambda$.

The stimulated emission cross section is another important parameter that provides interesting information about the laser performance of a material and can be easily determined from luminescence properties [29]. The spontaneous emission cross section between ${}^4F_{3/2} \rightarrow {}^4I_{J'}$ is represented by the equality [1, 13, 30]:

$$\sigma_{em}\left({}^4F_{3/2}\rightarrow {}^4I_{J'}\right) = \frac{\lambda_p^4}{8\pi\ c\ n\ \Delta\lambda_{\text{eff}}}A\left({}^4F_{3/2}\rightarrow {}^4I_{J'}\right), \quad (5)$$

where λ_p is the peak emission wavelength, c is the speed of light in a vacuum, n is the refractive index at each emission peak wavelength, and $\Delta\lambda_{\text{eff}}$ is the effective emission linewidth. The effective linewidth is used instead of the full width at half maximum linewidth because the emission band is asymmetric. This parameter is represented by [1, 12, 13, 30]: $\Delta\lambda_{\text{eff}}=\int I_{PL}(\lambda)d\lambda/I_{PL}^{\max}$. Here, $I_{PL}^{\max}$ is the maximum intensity at fluorescence emission peaks.

Once the radiative parameters are known, non-radiative losses and quantum efficiency can be determined. The quantum efficiency (η) is obtained from lifetime measurements: $\eta=\tau_{\exp}/\tau_R$. Here, $\tau_{\exp}$ is the experimental lifetime, and τ_R is the calculated lifetime from the Judd–Ofelt theory.

3 Experimental Procedure

Two sets of PANK matrices with nominal composition $40P_2O_5 \cdot 20Al_2O_3 \cdot 35Na_2O \cdot 5K_2O$ (in mole percent) were synthesized by the fusion method. These were undoped and doped with Nd^{3+} ions, resulting in PANK and PANK+$x$$Nd_2O_3$ (in weight percent), with x=1; 2; 3; 4; 5; 6. This glass system results from combining a network-forming oxide P_2O_5 with network modifier oxides Na_2O and K_2O and an intermediate oxide Al_2O_3. The P_2O_5 oxide is optically transparent and increases thermal stability. The Na_2O oxide reduces the melting point and increases glass system homogenization by reducing defects and bubbles. The Al_2O_3 and K_2O oxides are added to increase chemical resistance, reduce hydroxyl $(O–H)^-$ group density, and improve mechanical properties.

The powder was melted in porcelain crucibles and in a carbon-rich atmosphere for 30 min at 1,350 °C. The melt was then rapidly cooled between graphite plates in an oven at 250 °C. The resulting blades were heated at 350 °C for 48 h to partially remove internal stresses. The melt was manually rotated at least three times inside the crucible. This procedure was effective because the optical density absorption measurements, taken at various points during sample preparation,

demonstrate sample homogeneity. All of the samples underwent lengthy and meticulous polishing to minimize surface roughness (flat nanosurface) and make the sides parallel. The samples were also cleaned immediately prior to optical absorption (OA), photoluminescence (PL), and time-resolved photoluminescence (TRPL) measurements to avoid surface contamination. OA was determined using a Shimadzu UV-3600 spectrophotometer, and samples were excited by Ar^{+} (λ_{exc}=514 nm) and diode (λ_{exc}=532 nm) lasers for PL and TRPL spectra, respectively. A thermoelectrically cooled GaInAs pin photodiode and a standard lock-in technique were used to collect PL measurement spectra at NIR wavelengths. TRPL measurements were recorded using a digital phosphor oscilloscope (Tektronix DPO 2012, 100 MHz, 1 GS/s) and detected with a Si PIN photodiode operating in the photoconductive mode in the 200- to 1,100-nm range. All characterizations were performed at room temperature.

The ion density, N (ions per cubic centimeter), was evaluated by $N(\text{ions/cm}^3)=x\rho N_A/M$, where ρ is the density of the glass, N_A is Avogadro's number, x is the mole fraction of rare earth oxide, and M is the average molecular weight of the glass [12].

4 Results and Discussion

Figure 1 shows the absorbance and luminescence spectra of the PANK and PANK+$x$$Nd_2O_3$ (in weight percent) glass systems in the electromagnetic spectrum (Fig. 1a, UV–VIS–NIR; Fig. 1b, IR; and Fig. 1c, NIR spectral range). Allowed Nd^{3+} electronic transitions are visible in the UV–VIS–IR spectral range due to the high optical band-gap energy of the PANK glass system. For low Nd^{3+} concentrations, Fig. 1a shows that the optical band-gap energy red shifts with increasing Nd^{3+} concentrations (3.906 eV for x=0 and 3.826 eV for x=1 %). This shift probably occurs because the ionic radius of Nd^{3+} is higher relative to other elements in the glass, causing rearrangement of the glass structure. The optical density of the OH^{-} band in Fig. 1b is lower than in other vitreous systems such as SNAB (SiO_2–Na_2O–Al_2O_3–B_2O_3). The SNAB system has low quantum efficiency associated with the OH^{-} band [1]. This indicates that energy transfer from Nd^{3+} ion states to the OH^{-} band can be neglected in PANK and that the allowed electronic transition, $^4I_{9/2} \rightarrow {}^4I_{15/2}$, of the Nd^{3+} ions in PANK+$x$$Nd_2O_3$ (in weight percent) is more intense relative to the SNAB glass system [1]. This may result in a system with high quantum efficiency. Figure 1c shows the luminescence spectra of the Nd^{3+} ions in the PANK system at room temperature. Here, the shape of the bands at about 900 nm is modified as Nd_2O_3 concentration increases. This indicates that allowed Nd^{3+} electron transitions are influenced by the rearrangement of the system caused by Nd^{3+}.

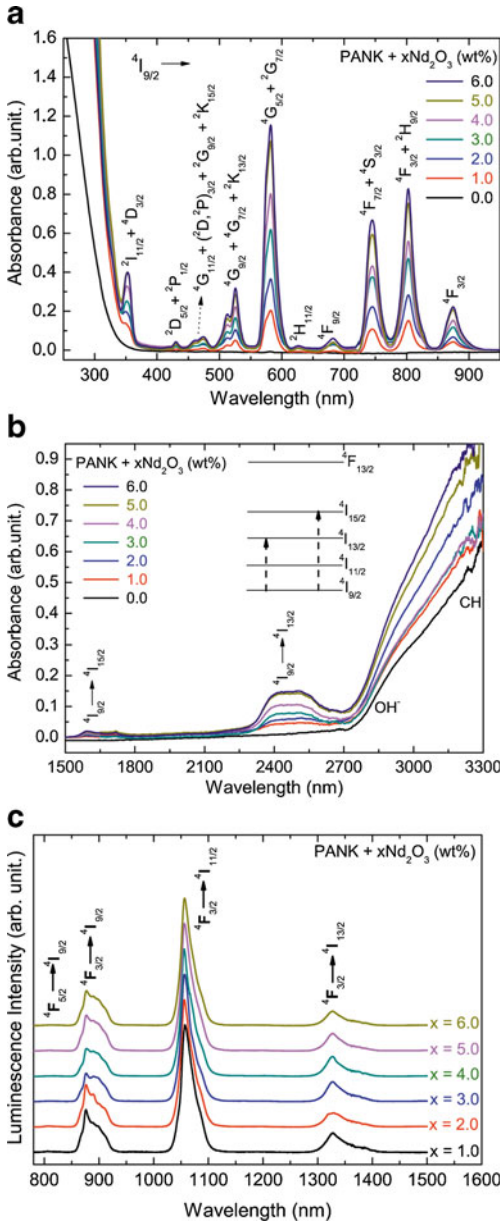

Fig. 1 Absorbance spectra of PANK and Nd^{3+} ions in the PANK system as a function of concentration of **a** UV and vis, **b** IR, and **c** luminescence spectra using $\lambda_{exc.}$=514.5 nm excitation

Figure 2 shows the behavior of the Judd–Ofelt intensity parameters ($\Omega_\lambda(\lambda=2, 4, 6)$) in the PANK glass system as a function of Nd^{+3}concentration. Relatively high Ω_2 values indicate that Nd^{3+} ions have greater asymmetric and covalent bonding. Ω_2 increases with Nd_2O_3 concentration, suggesting that Nd^{3+} modifies the glass network by increasing disorder. This in turn decreases the optical band gap of the PANK glass system (Fig. 1a). Thus, repulsive forces may arise between Nd ions and other adjacent cations that modify the glass network.

Nd^{3+} concentration also influences Ω_4 and Ω_6. The parameter Ω_4 is generally related to the long-range potential, while the Ω_6 can be related to the rigidity of the system, and its

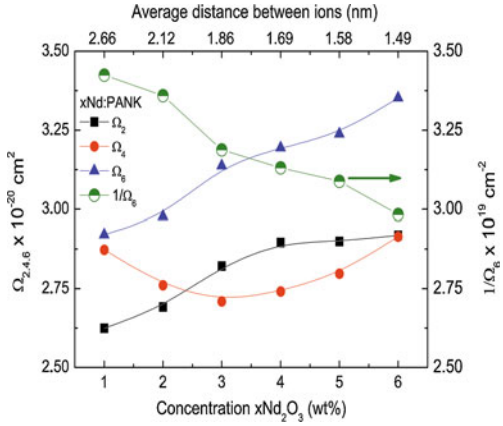

Fig. 2 Judd–Ofelt $\Omega_{2,4,6}$ and $1/\Omega_6$ parameters as function of Nd_2O_3 concentration in the PANK system

reciprocal value ($1/\Omega_6$) gives information on the ionicity around the RE^{3+} ions [31–33]. Increasing $\Omega_4$with rising Nd_2O_3 concentrations indicates possible far-reaching impacts on the host matrix in the vicinity of Nd–O [12, 33]. Low concentrations of Nd^{3+} ($0<x<3$) rearrange the network, which reduces these repulsive forces. High Nd^{3+} concentrations ($3\leq x\leq 6$) lead to a splitting of Nd^{3+} levels by a crystal field including the contributions from neighboring Nd^{3+} ions. This contributes to the increasing of the Ω_4 parameter. This behavior has been observed in other glass systems [33] and can be seen in the luminescence spectra (Fig. 1c) where the shape of the band centered at 900 nm is heavily modified as Nd_2O_3 (in weight percent) concentration increases from 2 to 3.

It is known that Ω_6 decreases as the mechanical rigidity of a system increases [1, 31, 32]. The Ω_6 of the PANK system (see Fig. 2) was higher than that observed in the SNAB system ($\Omega_6 \sim 0.8\times10^{-20}$ cm^2) [1]. Thus, PANK tends to be less rigid than SNAB and other glass systems (see Table 1). It is also known that the inverse of Ω_6 [1, 43, 44] is proportional to the ionicity of the ion in the ligand field [1, 43, 44]. Lower $1/\Omega_6$ values indicate a less ionic and more covalent bond. Figure 2 shows that $1/\Omega_6$ decreases as Nd_2O_3 concentration increases in the PANK glass system. In other words, Nd^{3+} ionicity decreases in the ligand field as Nd_2O_3 concentration increases in the glass system host. However, increasing concentration modifies the crystal field potential by breaking the surrounding symmetry (increasing Ω_2) and increasing ion covalence (see Table 1).

Figure 3 shows the calculated and experimental emission branching ratios or transition probabilities of allowed electronic transitions as a function of Nd^{3+} concentration. These experimental and calculated values are in good agreement. The probability of a $^4F_{3/2} \rightarrow {}^4I_{15/2}$ transition was estimated from the OA spectra. The result (0.35 %) suggests very low luminescence intensity from the $^4F_{3/2} \rightarrow {}^4I_{15/2}$ transition that was undetectable in the electromagnetic spectrum given equipment limitations.

Figure 4 shows the dependence of experimental and calculated fluorescence lifetime and quantum efficiency of the $^4F_{3/2}$ state with increasing Nd^{3+}concentration. Quantum efficiency was high (98 %) in the proposed Nd^{3+}-doped PANK glass system at low Nd^{3+} concentrations. It can be seen that both the fluorescence lifetime and quantum efficiency of the $^4F_{3/2}$ state decrease as Nd^{3+} concentration increases. The high quantum efficiency of the Nd^{3+}-doped PANK glass system was recently confirmed by the thermal lens technique [45].

It is known that non-radiative processes reduce the lifetime of radiative transitions. These processes are governed by energy transfers from RE ions to the host material (e.g., network vibrational modes, OH and CH radicals, and cross-relaxation process (ion–ion interaction)) [1]. The multiphonon relaxation rate [13, 46] for the $^4F_{3/2}$ level should be low, as will be shown later [1]. Thus, the short experimental lifetime of the samples at higher Nd^{3+} concentrations is probably due to excited energy migration between Nd^{3+} ions and, to a lesser extent, energy transfer to unintentionally introduced impurities and/or defects near the Nd^{3+} ions.

Considering the non-radiative transition processes from the $^4F_{3/2}$ Nd^{3+} level, namely resonant energy migration processes between Nd^{3+} ions (cross relaxation), it can be seen that resonance only occurs from $^4F_{3/2} \rightarrow {}^4I_{13/2}$ to $^4F_{3/2} \rightarrow {}^4G_{7/2}$, $^4F_{3/2} \rightarrow {}^4I_{11/2}$ to $^4F_{3/2} \rightarrow {}^4G_{11/2}$, and $^4F_{3/2} \rightarrow {}^4I_{9/2}$ to $^4F_{3/2} \rightarrow {}^2D_{11/2}$. The JO theory allows these transitions for Nd–Nd interactions. The distance between ions at low Nd concentrations is great and therefore does not allow interaction between dipoles [47–49]. As the distance between dipoles decreases, interactions between dipoles become stronger and RE ion concentration increases. The reduction in experimental lifetime of the $^4F_{3/2}$ state with increasing Nd_2O_3 concentration has been thoroughly studied by Stokowski using the empirical ratio [50]:

$$\tau_{\exp} = \frac{\tau_o}{1+(N/Q)^n} \tag{8}$$

where τ_o is the observed lifetime for a diluted system, Q is the Nd concentration at $\tau = \tau_o/2$, and n is an adjustable parameter. In glass doped with Nd^{3+}, n near two occurs when fluorescence quenching is dominated by cross-relaxation processes. A high Q value results in an optically efficient system. In the present study, good fit was obtained using $\tau_o = 385$ μs, $Q = 5.5$ Nd_2O_3 (weight percent) (approximately 2.5×10^{20} ions/cm^3), and $n = 1.8$ (dashed red line, Fig. 4). This indicates that PANK is similar to CANB ($52CaO \cdot 36A1_2O \cdot 6Na_2O \cdot 6BaO \cdot 0.5Nd_2O_3$), CANS ($52CaO \cdot 36A1_2O_3 \cdot 6Na_2O \cdot 6SrO \cdot 0.5Nd_2O_3$), LSCA ($47.4CaO \cdot (41.5-x)Al_2O_3 \cdot 7.0SiO_2 \cdot 4.1MgO$, where x varied from 0.5 to 5.0 (in weight percent)), ED-2 (Li–Ca–Al silicate commercial glasses—Owens-Illinois), and YAG (yttrium aluminum garnet) systems [6, 34, 36, 51–53]. The good fit and high n ($n \approx 2$) and Q parameters suggest that energy transfer is primarily due to cross relaxation.

Table 1 JO ($\times 10^{-20}$ cm^2) parameters, quantum efficiency (in percent), and stimulated emission section ($\times 10^{-20}$ cm^2) for various materials such as crystals, glass systems, films, and polymers with low Nd^{3+} concentrations

Host	Ω_2	Ω_4	Ω_6	Quantum efficiency	Emission section	Reference
CANB glass	4.46	5.18	2.73	80	1.32	[34]
CANS glass	3.71	5.03	2.90	75	1.32	[34]
CASGAR garnet	0.98	3.20	3.63	–	–	[35]
YAG:Nd^{3+} (single crystal)	0.20	2.70	5.00	96.1	100	[36, 37]
ED-2	3.30	4.68	5.18	78	2.71	[34]
LSCA	3.21	4.07	2.01	93	2.19	[6]
NYCaB10	4.66	10.34	10.32	–	–	[38]
PbO–Bi_2O_3–Ga_2O_3–BaO	3.2	2.7	3.1	80	–	[39]
Fluoroaluminate glass	1.97	3.43	5.38	–	–	[40]
Phosphate (KBAP)	3.42	4.09	4.35	60	2.3	[41]
Fluorophosphate (A)	2.57	4.40	5.99	41	3.69	[41]
Fluoride	1.21	2.54	4.19	40	1.87	[41]
Sulfide				36	–	[41]
Fluorophosphate (2 wt.%)	1.83	4.73	4.19	60	2.68	[41]
PMMA	2.11	3.78	2.61	–	–	[42]
PMMA	38	3.58	4.71	–	1.87	[42]
HEMA	7.78	4.26	7.19	–	–	[42]
POF	0.83	1.64	4.04	–	1.21	[42]
ZBLAN	2.66	3.05	4.08	–	2.9	[42]
YAG:Nd^{3+} (ceramic)	0.22	3.55	5.33	88.8	29.7	[36, 37]
YAG:Nd^{3+} (ceramic)	0.22	2.57	3.71	77.5	17.3	[36]
Poly(styrene sulfonate) (PSS) films	3.0	10.5	10.5	–	1.21	[42]
SNPZ	3.66	5.53	2.73	93	–	[30]
SNAB	1.2	2.3	0.8	25	1.2	[1]
SBP glass	1.0–2.0	0.5–1.6	0.8–2.4	–	1.0–3.0	[33]
SBP ceramic–glass	1.0–2.5	0.6–1.3	1.1–2.2	–	1.3–2.6	[33]
PANK	2.62	2.87	2.92	98	4.12	This work

The ratio ($^4F_{3/2} \rightarrow {}^4I_{13/2}$)/($^4F_{3/2} \rightarrow {}^4G_{7/2}$) is 0.99. This suggests a resonant system that allows energy transfer by cross relaxation. Other transitions occur at lower intensities because of lower energy ratios (e.g., 0.98 for the $^4F_{3/2} \rightarrow {}^4I_{11/2}$ to $^4F_{3/2} \rightarrow {}^4G_{11/2}$ transition and 0.97 for $^4F_{3/2} \rightarrow {}^4I_{9/2}$ to $^4F_{3/2} \rightarrow {}^2D_{11/2}$). The $^4F_{3/2} \rightarrow {}^4I_{13/2}$ transition probably has the greatest effect on luminescence quenching due to greater resonance.

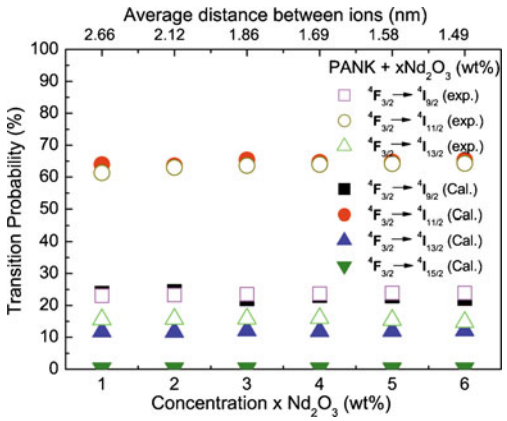

Fig. 3 Calculated and experimental probability of the allowed electronic luminescence transitions in the PANK system

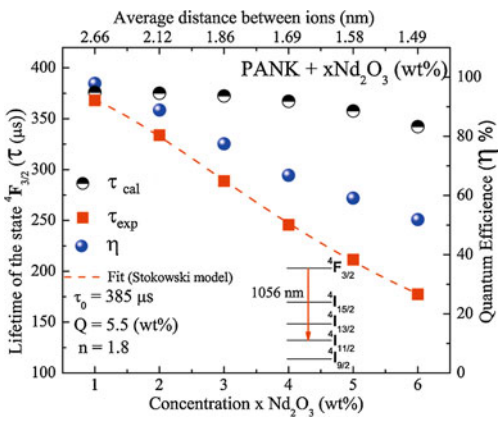

Fig. 4 Theoretical and experimental lifetime, and quantum efficiency, of the $^4F_{3/2}$ state of Nd^{3+} in the PANK system

As previously mentioned, energy transfer to OH^- and CH radicals via phonons exists in the vitreous network. The literature reports that phosphate-based glass systems have high vibrational modes [54] that also decrease experimental lifetime and quantum efficiency [30]. Infrared absorption measurements were performed to further investigate these hypotheses. Figure 1b shows the far-infrared spectra of the PANK glass system doped with different concentrations of Nd_2O_3. Here, very weak absorption is visible at approximately 2,790 nm (3,584 cm^{-1}), which is characteristic of OH^- radicals [55]. There also appears to be a band edge centered at 3,450 nm (2,900 cm^{-1}) that can be associated with the vibration mode of CH radicals [56]. The presence of these radicals in the PANK glass system causes energy transfers via non-radiative electronic transitions from Nd^{3+} ions that reduce experimental lifetime of the $^4F_{3/2}$ state [1]. This energy transfer mechanism is not so favored because energy differences between Nd^{3+} states do not have an integer number of phonons (see below) [13, 46].

Non-radiative transition losses are determined by considering that the total transition rate ($W_T=1/\tau_{exp}$) is the sum of the radiative rates ($W_R=1/\tau_R$) and all non-radiative (W_{NR}) mechanisms such as multiphonon decay, cross relaxation between Nd^{3+} ions, and energy transfer between Nd^{3+} ions and impurities (OH^- or CH radicals and other quenching centers). The inverse of the total transition rate corresponds to the inverse of experimental lifetime: $W_T=W_R+W_{NR}, \rightarrow W_{NR}=(1/\tau_{exp})-(1/\tau_{exp}), \rightarrow W_{NR}=(1/\tau_{exp})-(1/\tau_R)$. The multiphonon relaxation rate can be estimated by the empirical relation [13, 57]:

$$W_{NR} = W_{MP}(T) = C_p \frac{\exp[-\alpha \Delta E]}{\{1-\exp[\hbar\omega/(K_B T)]\}^p} \qquad (12)$$

where C_p and α are host-dependent non-radiative parameters, ΔE is the energy gap between two successive levels, and $p = \Delta E/(\hbar\omega)$ is the number of phonons emitted in the relaxation process. This process is more efficient when p is a small integer number. In borosilicate glass doped with Nd^{3+} ions, for example, the multiphonon emission process from the $^4F_{3/2}$ level to the $^4I_{13/2}$ level, $\Delta E = 7{,}519\ cm^{-1}$, requires approximately seven ($p = 7.09$) phonon emissions because the maximum phonon energy in borosilicate glass is $\hbar\omega = 1{,}060\ cm^{-1}$. Thus, the multiphonon relaxation rate for the $^4F_{3/2}$ level is expected to be low in borosilicate glass [1]. In our sample, the phonons emitted in the relaxation process corresponding to the $^4F_{3/2} \rightarrow {}^4I_{9/2}$, $^4F_{3/2} \rightarrow {}^4I_{11/2}$, and $^4F_{3/2} \rightarrow {}^4I_{13/2}$ transitions of Nd^{3+} ions are respectively, $p = 3.3$, 2.7, and 2.2 for OH^- phonons and $p = 3.9$, 3.2, and 2.6 for CH phonons. Thus, energy migration followed by quenching in OH^- and CH results in negligible lifetime reduction.

Pembertonet et al. [58] studied Raman spectra in metaphosphate glasses and found a medium-to-strong intensity band at 690–700 cm^{-1} for the ν_s(POP) vibration, a strong band at 1,178–1,168 cm^{-1} for the $\nu_s(PO_2)$ vibration, and a medium-to-weak band at 1,260–1,280 cm^{-1} for the $\nu_{as}(PO_2)$ vibration. The positions of these bands are sensitive to phosphate chain length. In particular, the somewhat more intense peak at approximately 1,160 cm^{-1} is due to symmetric stretching of the nonbridging oxygen in Q_2 phosphate groups [59]. The same mechanism for energy transfer to the OH^- and CH radicals is valid for the network vibration in which the $^4F_{3/2} \rightarrow {}^4I_{9/2}$, $^4F_{3/2} \rightarrow {}^4I_{11/2}$, and $^4F_{3/2} \rightarrow {}^4I_{13/2}$ transitions of the Nd^{3+} ions correspond, respectively, to $p = 9.8$, 8.2, and 6.5 of the most intense vibrational mode of the phosphate glasses.

In summary, our results demonstrate that luminescence transitions of the Nd^{3+} ions are not resonant with the vibrational modes of the network and OH^- and CH radicals, and explain the high efficiency of the PANK glass system doped with Nd^{3+} ions. This is due to the low rate of energy transfer to vibrational modes of the glass network and OH^- and CH radicals. Ion–ion interactions are responsible for reductions in experimental lifetime as Nd concentration increases (as in Stokowski's model) [50]. The highest efficiency value, at the lowest Nd^{3+} ion concentration, is comparable to that of the YAG:Nd^{3+} crystal [36], [37] (Table 1). For example, quantum efficiency varies from 45 to 60 % at concentrations up to 2 mol% in LiFP and BaFP glass fluorophosphates [60]. This suggests that the PANK system is a strong candidate for laser device applications.

The stimulated emission cross section provides useful information about the potential laser performance of a material and can be easily evaluated using luminescence properties [29]. Its value signifies the rate at which energy is extracted from the lasing material. Previous studies [61] have

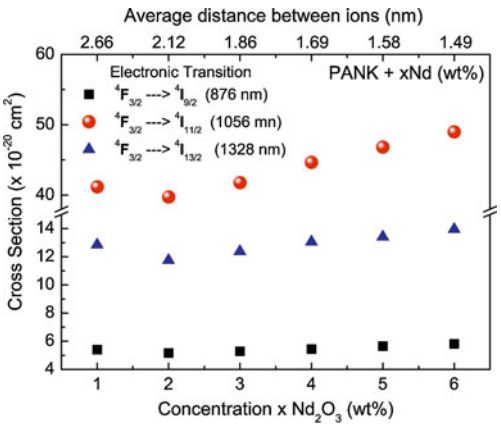

Fig. 5 Stimulated emission section of the allowed electronic transitions ($^4F_{3/2} \rightarrow {}^4I_{9/2,11/2,13/2}$) as a function of Nd_2O_3 concentration in the PANK system

shown that the stimulated emission cross section can increase as the refractive index of a glass host increases. This change is due to increases in the electric dipole transition of rare earth ions as the refractive index of the glass host increases. Good laser transitions are characterized by large stimulated emission cross sections [22, 41, 62]. Figure 5 shows a section of the stimulated emission, $\sigma(^4F_{3/2} \rightarrow {}^4I_{J'})$, as a function of Nd_2O_3 concentration in the PANK glass system. The sequence of these section values is $\sigma(^4F_{3/2} \rightarrow {}^4I_{11/2}) > \sigma(^4F_{3/2} \rightarrow {}^4I_{13/2}) > \sigma(^4F_{3/2} \rightarrow {}^4I_{9/2})$. The $^4F_{3/2} \rightarrow {}^4I_{11/2}$ section is somewhat dependent on concentration. In this case, the $\sigma(^4F_{3/2} \rightarrow {}^4I_{11/2})$ section of the Nd^{3+} ions varies between 40 and 50×10^{-21} cm^2. These values are near those of other systems at concentrations up to 2 mol% (e.g., LiFP $\sigma(^4F_{3/2} \rightarrow {}^4I_{11/2}) = 67 \times 10^{-21}$ cm^2 and commercially available fluorophosphate laser glass L-223 $\sigma(^4F_{3/2} \rightarrow {}^4I_{11/2}) = 35 \times 10^{-21}$ cm^2) [60] (Table 1). The mechanism promoting stimulated emissions becomes more efficient when the distance between identical ions decreases. Peak cross sections are dependent on intensity parameters, Ω_λ, and the bandwith, $\Delta\lambda_{eff}$. Both are affected when composition changes. The effective bandwidth is a measure of the overall extent of the Starks splitting of the J manifolds and is inhomogeneous due to the site-to-site variations in the local fields with which the rare earth ion interacts.

5 Conclusions

Nd^{3+} ions embedded in a PANK phosphate glass system were synthesized by the fusion method. Optical properties of this system were studied by optical absorption, photoluminescence, and lifetime measurements. Judd–Ofelt parameters, radiative rates, lifetime, branching ratios, and the emission cross section were calculated. Quantum efficiency of the Nd^{3+}-doped PANK glass system is high (98 %) at low Nd^{3+} concentrations. Additionally, fluorescence lifetime and quantum efficiency of the $^4F_{3/2}$ state decrease as Nd^{3+} concentration increases.

At the lowest concentration (1 % Nd^{3+}), quantum efficiency is highest and comparable to that of a YAG:Nd^{3+} crystal. The stimulated emission section of Nd^{3+}-doped PANK glass is higher than other glass and crystal systems, making it an attractive option for the optical cavities of highly efficient laser systems. Reduction in the experimental lifetime of the $^4F_{3/2} \rightarrow {}^4I_{11/2}$ transition with increasing Nd_2O_3 concentration was attributed to non-radiative energy transfer by cross relaxation between Nd^{3+} ions and phonon charge losses to the glass network. Non-radiative energy transfer from Nd^{3+} ions to OH^- and CH radicals can be disregarded because $^4F_{3/2} \rightarrow {}^4I_{11/2}$ electronic transition energy does not correspond with the vibration frequency multiples of these radicals. Finally, it was concluded that cross relaxation also decreases the lifetime of the $^4F_{3/2}$ Nd^{3+} level. We believe that these results may inspire further investigation and possible device applications.

Acknowledgments The authors are grateful for financial support from CAPES, CNPq, and FAPEMIG.

References

1. E.O. Serqueira, N.O. Dantas, M.J.V. Bell, Control of spectroscopic fluorescence parameters of Nd^{3+} ions as a function of concentration in a SiO_2–Na_2O–Al_2O_3–B_2O_3 glass system. Chem. Phys. Lett. **508**, 125–129 (2011)
2. Y. Xu, S. Li, L. Hu, W. Chen, Effect of copper impurity on the optical loss and Nd^{3+} nonradiative energy loss of Nd-doped phosphate laser glass. J. Rare Earths **29**, 614–617 (2011)
3. Y. Nageno, H. Takebe, K. Morinaga, Correlation between radiative transition probabilities of Nd^{3+} and composition in silicate, borate, and phosphate glasses. J. Am. Ceram. Soc. **76**, 3081–3086 (1993)
4. A.R. Devi, C.K. Jayasankar, Optical properties of Nd^{3+} ions in lithium borate glasses. Mater. Chem. Phys. **42**, 106–119 (1995)
5. V. Mehta, G. Aka, A.L. Dawar, A. Mansingh, Optical properties and spectroscopic parameters of Nd^{3+}-doped phosphate and borate glasses. Opt. Mater. **12**, 53–63 (1999)
6. E. Pecoraro, J.A. Sampaio, L.A.O. Nunes, S. Gama, M.L. Baesso, Spectroscopic properties of water free Nd_2O_3-doped low silica calcium aluminosilicate glasses. J. Non-Cryst. Solids **277**, 73–81 (2000)
7. E. Brown, C.B. Hanley, U. Hömmerich, A.G. Bluiett, S.B. Trivedi, Spectroscopic study of neodymium doped potassium lead bromide for mid-infrared solid state lasers. J. Lumin. **133**, 244–248 (2013)
8. R.M. Macfarlane, F. Tong, A.J. Silversmith, W. Lenth, Violet cw neodymium upconversion laser. Appl. Phys. Lett. **52**, 1300–1302 (1988)
9. A. Flórez, J.F. Martínez, M. Flórez, P. Porcher, Optical transition probabilities and compositional dependence of Judd–Ofelt parameters of Nd^{3+} ions in fluoroindate glasses. J. Non-Cryst. Solids **284**, 261–267 (2001)
10. K. Arai, H. Namikawa, K. Kumata, T. Honda, Y. Ishii, T. Handa, Aluminum or phosphorus co-doping effects on the fluorescence and structural-properties of neodymium-doped silica glass. J. Appl. Phys. **59**, 3430–3436 (1986)
11. S.A. Lourenco, N.O. Dantas, E.O. Serqueira, W.E.F. Ayta, A.A. Andrade, M.C. Filadelpho, J.A. Sampaio, M.J.V. Bell, M.A. Pereira-da-Silva, Eu3+ photoluminescence enhancement due to thermal energy transfer in Eu_2O_3-doped SiO_2-B_2O_3-PbO_2 glasses system. J. Lumin. **131**, 850–855 (2011)
12. S. Mohan, K.S. Thind, G. Sharma, Effect of Nd^{3+} concentration on the physical and absorption properties of sodium-lead-borate glasses. Braz. J. Phys. **37**, 1306–1313 (2007)
13. C. Venkateswarlu, Y.C. Ratnakaram, M. Seshadri, D.T. Naidu, Spectral investigations on Ho^{3+} doped mixed alkali chloroborate glasses. Braz. J. Phys. **41**, 281–289 (2011)
14. M.C. Silva, F.H. Cristovan, R. Ruggiero, W.O. Cruz, A. Marletta, Near-infrared emission of Nd-PSS films. Braz. J. Phys. **36**, 499–500 (2006)
15. L.R.P. Kassab, R.D. Mansano, L.D. Zambom, V.D. Del Cacho, Semiconductor characteristics of Nd doped PbO-Bi_2O_3-Ga_2O_3 films. Braz. J. Phys. **36**, 451–454 (2006)
16. B.R. Judd, Optical absorption intensities of rare-earth ions. Phys. Rev. **127**, 750–761 (1962)
17. G.S. Ofelt, Intensities of crystal spectra of rare-earth ions. J. Chem. Phys. **37**, 511–520 (1962)

18. W.T. Carnall, P.R. Fields, K. Rajnak, Electronic Energy Levels in Trivalent Lanthanide Aquo Ions.I. Pr3+ Nd3+ Pm3+ Sm3+ Dy3+ Ho3+ Er3+ and Tm3+. J. Chem. Phys. **49**, 4424 (1968)
19. W.T. Carnall, P.R. Fields, B.G. Wybourne, Spectral intensities of trivalent lanthanides and actinides in solution I Pr^{3+}, Nd^{3+}, Er^{3+}, Tm^{3+}, and Yb^{3+}. J. Chem. Phy. **42**, 3797 (1965)
20. H. Crosswhite, W.T. Carnall, and H.M. Crosswhite, Energy level structure and transition probabilities in the spectra of the trivalent lanthanides in LaF3, in, Argonne National Laboratory Report (1978)
21. A. Agarwal, I. Pal, S. Sanghi, M.P. Aggarwal, Judd-Ofelt parameters and radiative properties of Sm^{3+} ions doped zinc bismuth borate glasses. Opt. Mater. **32**, 339–344 (2009)
22. M. Seshadri, K.V. Rao, J.L. Rao, K.S.R.K. Rao, Y.C. Ratnakaram, Spectroscopic investigations and luminescence spectra of Nd^{3+} and Dy^{3+} doped different phosphate glasses. J. Lumin. **130**, 536–543 (2010)
23. C.K. Jørgensen, *Modern Aspects of Ligand Field Theory* (North-Holland Pub. Co., Amsterdam, 1971)
24. R. Reisfeld, Radiative and nonradiative transition of rare earths in glasses. Struct. Bond. **22**, 123–175 (1975)
25. R. Reisfeld, C.K. Jørgensen, *Lasers and Excited States of Rare Earths* (Springer, Berlin, 1977)
26. A. Mech, Crystal structure and optical of novel (N(C2H5)(4))[Nd(hfa)(4)(H2O)] tetrakis complex. Polyhedron **27**, 393–405 (2008)
27. A.J. Freeman, R.E. Watson, Theoretical investigation of some magnetic and spectroscopic properties of rare-earth ions. Phys. Rev. **127**, 2058–2075 (1962)
28. P. Nemec, J. Jedelsky, M. Frumar, M. Munzar, M. Jelinek, J. Lancok, On the optical properties of amorphous Ge-Ga-Se films prepared by pulsed laser deposition. J. Non-Cryst. Solids **326**, 53–57 (2003)
29. J.S. Wang, E.M. Vogel, E. Snitzer, Tellurite glass: a new candidate for fiber devices. Opt. Mater. **3**, 187–203 (1994)
30. E.O. Serqueira, N.O. Dantas, A.F.G. Monte, M.J.V. Bell, Judd Ofelt calculation of quantum efficiencies and branching ratios of Nd^{3+} doped glasses. J. Non-Cryst. Solids **352**, 3628–3632 (2006)
31. R. Reisfeld, G. Katz, C. Jacoboni, R. De Pape, M.G. Drexhage, R.N. Brown, C.K. Jørgensen, The comparison of calculated transition probabilities with luminescence characteristics of erbium(III) in fluoride glasses and in the mixed yttrium-zirconium oxide crystal. J. Solid State Chem. **48**, 323–332 (1983)
32. C.K. Jorgensen, R. Reisfeld, Judd-Ofelt parameters and chemical bonding. J. Less-Common Metals **93**, 107–112 (1983)
33. N.O. Dantas, E.O. Serqueira, M.J.V. Bell, V. Anjos, E.A. Carvalho, S.A. Lourenço, M.A. Pereira-da-Silva, Influence of crystal field potential on the spectroscopic parameters of SiO_2 B_2O_3 PbO glass doped with Nd_2O_3. J. Lumin. **131**, 1029–1036 (2011)
34. E.V. Uhlmann, M.C. Weinberg, N.J. Kreidl, L.L. Burgner, R. Zanoni, K.H. Church, Spectroscopic properties of rare-earth-doped calcium-aluminate-based glasses. J. Non-Cryst. Solids **178**, 15–22 (1994)
35. D.K. Sardar, S. Vizcarra, M.A. Islam, T.H. Allik, E.J. Sharp, A.A. Pinto, Spectroscopic analysis and the effects of color-centers on the laser performance of Nd^{3+} CaZn2y2Ge3o(12). Opt. Mater. **3**, 257–263 (1994)
36. D.K. Sardar, R.M. Yow, J.B. Gruber, T.H. Allik, B. Zandi, Stark components of lower-lying manifolds and emission cross-sections of intermanifold and inter-stark transitions of Nd^{3+} (4f3) in polycrystalline ceramic garnet Y3Al5O12. J. Lumin. **116**, 145–150 (2006)
37. G.A. Kumar, J.R. Lu, A.A. Kaminskii, K.I. Ueda, H. Yagi, T. Yanagitani, N.V. Unnikrishnan, Spectroscopic and stimulated emission characteristics of Nd^{3+} in transparent YAG ceramics. IEEE J. Quantum Electron. **40**, 747–758 (2004)
38. D.R.S. Santos, C.N. Santos, A.S.S. de Camargo, W.F. Silva, W.Q. Santos, M.V.D. Vermelho, N.G.C. Astrath, L.C. Malacarne, M.S. Li, A.C. Hernandes, A. Ibanez, C. Jacinto, Thermo-optical characteristics and concentration quenching effects in Nd($^{3+}$)doped yttrium calcium borate glasses. J Chem Phys **134**, 124503 (2011)
39. L.R.P. Kassab, N.D.R. Junior, S.L. Oliveira, Laser spectroscopy of Nd ($^{3+}$)-doped PbO-Bi2O3-Ga2O3-BaO glasses. J. Non-Cryst. Solids **352**, 3224–3229 (2006)
40. D. Piatkowski, Simulation of the absorption spectrum of Nd^{3+} activated fluoroaluminate glass. J. Non-Cryst. Solids **353**, 1017–1022 (2007)
41. J.H. Choi, A. Margaryan, A. Margaryan, F.G. Shi, Judd-Ofelt analysis of spectroscopic properties of Nd^{3+}-doped novel fluorophosphate glass. J. Lumin. **114**, 167–177 (2005)
42. M.C. Silva, F.H. Cristovan, C.M. Nascimento, M.J.V. Bell, W.O. Cruz, A. Marletta, Judd-Ofelt analysis of Nd^{3+} ions in poly(styrene sulfonate) films. J. Non-Cryst. Solids **352**, 5296–5300 (2006)
43. S. Tanabe, Optical transitions of rare earth ions for amplifiers: how the local structure works in glass. J. Non-Cryst. Solids **259**, 1–9 (1999)
44. A.J.G. Ellison, P.C. Hess, Lanthanides in silicate-glasses—a vibrational spectroscopic study. J Geophys Res-Solid **95**, 15717–15726 (1990)
45. A.A. Andrade, V. Pilla, S.A. Lourenço, A.C.A. Silva, N.O. Dantas, Fluorescence quantum efficiency dependent on the concentration of Nd^{3+} doped phosphate glass. Chem. Phys. Lett. **547**, 38–41 (2012)
46. T. Miyakawa, D.L. Dexter, Phonon sidebands, multiphonon relaxation of excited states, and phonon-assisted energy transfer between ions in solids. Phys. Rev. B **1**, 2961–2969 (1970)
47. T. Forster, Zwischenmolekulare Energiewanderung Und Fluoreszenz. Ann Phys-Berlin **2**, 55–75 (1948)
48. D.L. Dexter, A theory of sensitized luminescence in solids. J. Chem. Phys. **21**, 836–850 (1953)
49. M. Inokuti, F. Hirayama, Influence of energy transfer by exchange mechanism on donor luminescence. J. Chem. Phys. **43**, 1978–1989 (1965)
50. M.J.F. Digonnet, *Rare-earth-doped fiber lasers and amplifiers, revised and expanded* (CRC Press, Boca Raton, 2001)
51. W.F. Krupke, Radiative transition probabilities within 4f3 ground configuration of Nd-Yag. IEEE J. Quantum Elect. Qe **7**, 153–159 (1971)
52. A. Rosencwaig, E.A. Hildum, Nd-$^{3+}$ fluorescence quantum-efficiency measurements with photo-acoustics. Phys Rev B **23**, 3301–3307 (1981)
53. G.A. Kumar, L. Jianren, A.A. Kaminskii, K.I. Ueda, H. Yagi, T. Yanagitani, N.V. Unnikrishnan, Spectroscopic and stimulated emission characteristics of Nd < sup > 3 + </sup > in transparent YAG ceramics. Quantum Electronics, IEEE J. **40**, 747–758 (2004)
54. M. Elisa, I.C. Vasiliu, C.E.A. Grigorescu, B. Grigoras, H. Niciu, D. Niciu, A. Meghea, N. Iftimie, M. Giurginca, H.J. Trodahl, M. Dalley, Optical and structural investigation on rare-earth-doped aluminophosphate glasses. Opt. Mater. **28**, 621–625 (2006)
55. Q.H. Nie, X.J. Li, S.X. Dai, T.F. Xu, Z.J. Jin, X.H. Zhang, Investigation of concentration quenching and 1.3 mu m emission in Nd^{3+}-doped bismuth glasses. Spectrochim Acta A **70**, 537–541 (2008)
56. J.L. Kropp, M.W. Windsor, Luminescence and energy transfer in solutions of rare-earth complexes. I. Enhancement of fluorescence by deuterium substitution. J Chem Phys **42**, 1599 (1965)
57. D. Chen, Y. Wang, Y. Yu, E. Ma, F. Liu, Fluorescence and Judd–Ofelt analysis of Nd^{3+} ions in oxyfluoride glass ceramics containing CaF2 nanocrystals. J. Phys. Chem. Solids **68**, 193–200 (2007)
58. J.E. Pemberton, L. Latifzadeh, J.P. Fletcher, S.H. Risbud, Raman-spectroscopy of calcium-phosphate glasses with varying Cao modifier concentrations. Chem. Mater. **3**, 195–200 (1991)

59. M.G. Donato, M. Gagliardi, L. Sirleto, G. Messina, A.A. Lipovskii, D.K. Tagantsev, G.C. Righini, Raman optical amplification properties of sodium-niobium-phosphate glasses, Appl Phys Lett, 97 (2010).
60. G.A. Kumar, E. De la Rosa-Cruz, K. Ueda, A. Martinez, O. Barbosa-Garcia, Enhancement of optical properties of Nd^{3+} doped fluorophosphate glasses by alkali and alkaline earth metal co-doping. Opt. Mater. **22**, 201–213 (2003)
61. B.F. Aull, H.P. Jenssen, Vibronic interactions in Nd-Yag resulting in nonreciprocity of absorption and stimulated-emission cross-sections. IEEE J. Quantum Electron. **18**, 925–930 (1982)
62. Y.C. Ratnakaram, R.P.S. Chakradhar, K.P. Ramesh, J.L. Rao, J. Ramakrishna, The effect of host glass on optical absorption and fluorescence of $Nd(^{3+})$ in xNa(2)O-(30-x)K(2)O-70B(2)O(3) glasses. J. Phys. Condens. Matter **15**, 6715–6730 (2003)